MASS LOSS IN AGB STARS

M. GUÉLIN, R. LUCAS, AND R. NERI
Institut de Radioastronomie Millimétrique
300 rue de la Piscine, F-38406 Saint Martin d'Hères, France

Abstract. The phase of high mass loss, one of the ultimate phases of stellar evolution, is still poorly known. For a long time, large visual extinctions and small angular sizes have impeded the study of the most interesting objects in this stage. The recent development of mm and IR interferometry has allowed a breakthrough in this domain. Expelled molecules and dust are now routinely mapped at arcsecond resolutions, providing a large data base to which model predictions are confronted.

1. Mass loss rates

The main component of the expelled gas, molecular hydrogen, is hard to detect. Envelope masses and mass loss rates are therefore derived primarily from the observation of the two most stable trace components, CO and dust: CO, at 4.6 and 2.3 μm (mostly) in absorption and at mm wavelengths in emission; dust in emission throughout the IR-submm window.

In order to derive the H_2 mass from CO, one has to model the CO chemistry. This has been done in particular by Mamon et al. (1988, hereafter MGH), who first introduced accurate CO photodissociation cross sections in their chemical network. In the case of cold red giants ($T_* < 3000$K), the far UV photons come from interstellar space; their energy distribution can be described in terms of an attenuated 'standard interstellar radiation field' (or 'ISRF'). The IS radiation is absorbed by the dust grains as well as by the H_2 and CO molecules present in the outer envelope layers. In MGH's model, efficient CO self-shielding and shielding by H_2 lines make the CO fractional abundance relative to H_2, x(CO), follow almost a step function. It drops from $x(\mathrm{CO}) = \mathrm{few}\ 10^{-4}$, to almost zero as soon as the gas overpasses a critical 'photodissociation' radius R_{ph}.

Obviously, R_{ph} depends on the intensity of the local ISRF and on the mass loss rate, $\dot{M}$. In a more subtle way, it also depends on the dust grain properties. Olofsson et al. (1993), following MGH have derived a simple relation between

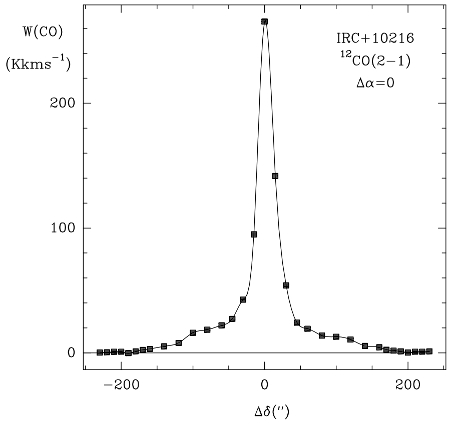

Figure 1: ^{12}CO J=2–1 line emission, integrated over the central 13 km s^{-1} velocity interval, along a strip passing through IRC+10216.

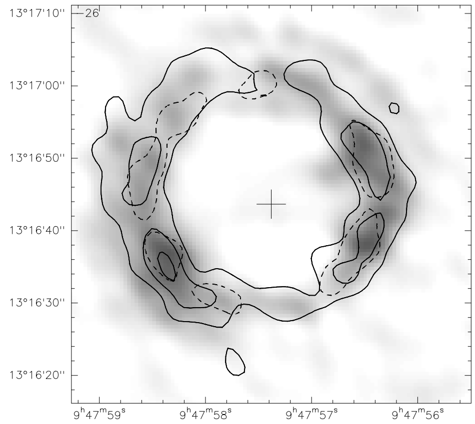

Figure 2: The C_3H (dashed) and C_4H (solid) contours of Fig. 4, superimposed on the C_2H brightness distribution (grey scale).

$R_{\rm ph}$ and $\dot{M}$ in the case of a constant isotropic mass loss rate and a 'standard' ISRF:

$$R_{\rm ph} = 4\,10^{16} \left(\frac{\dot{M}}{10^{-6}}\right)^{0.6} \left(\frac{v_{\rm exp}}{15}\right)^{-0.5} \left(\frac{x({\rm CO})}{3\,10^{-4}}\right)^{0.5} \ {\rm cm},$$

where $\dot{M}$ is in $M_\odot$ yr^{-1} and $v_{\rm exp}$, the expansion velocity, in km s^{-1}.

Figure 1 shows the ^{12}CO, J= 2–1 line profile along an EW cut passing through CW Leo/IRC+10216. CW Leo, the archetype of carbon stars, located only $D \sim 200$ pc from the Sun, is believed to have reached the very end of the AGB phase and to be just on the verge of evolving toward the PN phase (Guélin et al. 1993 –hereafter GLC– Kastner et al. 1994). It is surrounded by a thick envelope of dust and gas with a very rich chemistry. The CO profile shows a central 'core' and a broad 'plateau' whose intensity drops briskly at $R \simeq 120''$. Setting $R_{ph} = 120'' \simeq 3.5\,10^{17}$ cm, equation (1) yields $4\,10^{-5}$ $M_\odot$ yr^{-1}.

The CO profile of Fig. 1 obviously contains more information than the value of $R_{\rm ph}$. Truong-Bach & Rieu (1991) fitted all the CO mm data available for the central $R < 1'$ region of IRC+10216 with a radiative transfer code. They find a mass loss rate of $\dot{M} = 2.5\,10^{-5}$ $M_\odot$ yr^{-1} for the 'core' and $4\,10^{-5}$ $M_\odot$ yr^{-1} for the 'halo': the mass loss rate seems thus to have decreased by about a factor of 2 in the last 10^3 yr. A modelling of the innermost part of the IRC+10216 envelope has been made by Sahai & Wannier (1985) and Keady et al. (1988) on the basis of the IR data. Keady et al. derive the radial dust and gas temperature profiles as well as a velocity profile (the expansion velocity increases by steps from $V_e = 2$ to 14 km s^{-1}). They find for x(CO)= $3\,10^{-4}$ a mass loss rate of 4 10^{-5} $M_\odot$ yr^{-1}.

The observation of the dust thermal emission offers another way of studying mass loss rates. There, one has to assume a dust absorption coefficient and a dust-to-gas mass ratio (see, e.g., Walmsley et al. 1991). In the case of IRC+10216, Ridgway & Keady (1988) derive from interferometric 1.6–5.0 μm observations a *dust* mass loss of $2\,10^{-7}$ M$_\odot$ yr^{-1}, surprisingly small, in view of the above.

A comprehensive study of IRC+10216's continuum emission was made recently by Winters et al. (1994), who modelled in a self-consistent way: *i)* the formation of the dust grains by nucleation, *ii)* their acceleration by radiation pressure, and *iii)* their thermal equilibrium in the radiation field, taking into account grain-gas collisions. The stellar parameters were adjusted to fit the observed continuum spectrum from the near- to the far-IR, the expansion velocity, and the size (measured by IR interferometry) of the continuum source. Winters et al. arrive at a mass loss rate of $\dot{M} = 8\,10^{-5}$ M$_\odot$ yr^{-1}, an envelope mass $>$ 0.5 M$_\odot$ and a carbon-to-oxygen ratio of 1.3–1.5. The central star has presently a mass of 0.7 M$_\odot$, a surface temperature of 2000 K and a peak bolometric luminosity of $2.3\,10^4$ L$_\odot$, which yields a distance D = 170 pc. Of course, these values are only a set of possible solutions. They illustrate, nevertheless, how much can be derived from a well studied source.

There are not many AGB stars where such a wealth of observations is available. In most cases, one has to rely on coarse CO and/or IR continuum observations to estimate the mass loss rates. To date several hundreds of circumstellar envelopes have been detected in CO (see, e.g., the compilation by Loup et al. 1993), but for the vast majority of them only a single spectrum (e.g., ^{12}CO J= 2–1) is available. A crude idea of their mass loss rates can nevertheless be obtained from the relation between the CO integrated line intensity and the mass loss rate derived by Knapp & Morris (1985) and Kastner (1992) for optically thick envelopes. The distances of most objects being unknown, they are crudely evaluated from the IR and FIR fluxes by assuming AGB stars have bolometric luminosities $\simeq 10^4$ L$_\odot$ (see, e.g., Loup et al. 1993 for a more detailed discussion).

With the advent of powerful mm interferometers, it now becomes possible to map the CO emission of many circumstellar envelopes and directly measure their radial profile, size, and degree of asymmetry. This latter parameter is very important (and so far poorly known), since the first step in the evolution from AGB to PPN and PN is a disruption of the spherically symmetrical shell. (Such a disruption has just started in IRC+10216 – see Fig. 2 and GLC.)

The survey of a sample of 50 AGB and post-AGB stars has started at IRAM, and a first atlas, consisting of ^{12}CO J= 2–1 line emission maps, observed with the 30-m telescope, and of J=1–0 maps, resulting from a combination of 30-m telescope and the Bure interferometer data, is already available (Neri et al. *submitted*). The basic kinematical parameters, as well as the visibility curves,

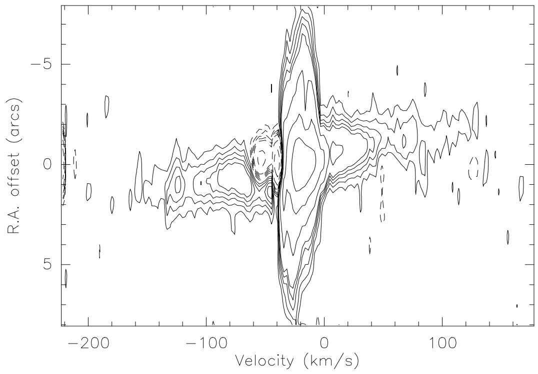

Figure 3: Position-velocity diagram along the EW high velocity outflow of the PPN CRL 618, observed in ^{12}CO J=1–0 line with a 2″ angular resolution (IRAM interferometer, Neri et al. *in preparation*).

envelope sizes, and degrees of asymmetry are given for all objects. The CO visibilities are typical of Gaussian CO line brightness radial distributions. They show no evidence of a sharp photodissociation cutoff at the (limited) sensitivity of the present data. Only a few envelopes are found to be strongly asymmetrical. Most stars, however, were only observed with the interferometer in the 'snapshot' mode with poor uv coverage, so that weak asymmetries could have been missed.

2. Pre-Planetary Nebulae

Among the objects showing strong asymmetries, are the well known post-AGB stars M1–92 and CRL 618, both of which exhibit high velocity (HV) molecular outflows. These outflows and the central cores of the envelopes were mapped in the ^{12}CO (1–0) line with a good uv coverage and high sensitivity using the Bure interferometer. In both objects there is a clear interaction between the outflow and the core material. The results on M1–92 were already reported by Bujarrabal et al. (1994). The core-outflow interaction in CRL 618 is illustrated in Fig. 3, where we show the position-velocity diagram observed along the outflow E–W axis of symmetry. The slowly expanding core appears as a bright, slightly bipolar source, extending between $\pm7''$ in R.A. and -40 and 0 km s^{-1} in velocity. The HV outflow is also bipolar; it is visible from -180 to $+140$ km s^{-1}. The gas at large positive velocities arises from distinct impact regions, unresolved by the 2″ (FWHP) synthesized beam and located 1–2″ W of the central source. That at negative velocities seems less collimated: it extends from 2″ E until right in front of the continuum source, as attested by the absorption visible between -40 and -80 km s^{-1}. Both the core and the HV CO data can be explained by the schematic model of CRL 618 proposed by Neri et al. (1992) on the basis of HCN (1–0) interferometric observations. Other species mapped in CRL 618 are ^{13}CO (Yamamura et al. 1994), CS (Hajian et al. 1995b) and NH_3 (Martin-Pintado et al. 1995).

3. Chemistry

While matter is expelled from the stellar atmosphere and expands into outer space, it assumes a wide range of physical conditions. The density decreases by several orders of magnitude and the temperature drops from thousands of K to a mere 10–20 K. In the process, about every molecule formation/destruction mechanism occurs: 3-body reactions in the hot atmosphere, grain condensation in the upper atmospheric layers, ion–molecule and radical–molecule reactions in the circumstellar envelope, and photodissociation in the envelope outer 'skin'. All of this makes an exceptionally rich chemistry, as attested by the more than 50 molecular species identified in IRC+10216.

The simple geometry and velocity field of AGB star envelopes is another asset. It allows to determine the physical conditions and dynamical timescales and makes it possible to follow in time the chemical processes by measuring the molecular abundances at different radii. Such studies, however, require linear resolutions reachable only in the closest objects. IRC+10216, $\simeq$ 200 pc away, is obviously a prime target.

The chemistry in the envelope is far from thermodynamic equilibrium, as illustrated by the large abundance of radicals (e.g., $x(\mathrm{CP}) > x(\mathrm{HCP})$), and is highly time dependent. The short dynamical time scales (in IRC+10216, it takes 10^4 yr for the matter ejected by the central star to cross the entire CO envelope) imply that chemical processes must be fast. The formation of dust grains, which removes from the gas most elements heavier than carbon; photodissociation, which breaks out molecules into small radicals and atoms; photoionization and ionization by cosmic rays, which produce C^+, $C_2H_2^+$,...; and, finally, fast neutral and ion–molecule reactions shape the molecular composition. It is also likely that grain chemistry plays a role in the final composition, all the more that the dust grains, while drifting outwards, are exposed to an increasingly large UV intensity.

The most recent models of gas phase chemistry in CSEs (with particular emphasis on IRC+10216) are those of Glassgold and co-workers (see Cherncheff et al. 1993 and references therein) and Millar & Herbst (1994). In addition to the photodissociation and ion–molecule reactions already present in previous models, they include neutral reactions, such as radical–radical reactions. Although neutral reactions have smaller rate coefficients than the fast ion–molecule reactions, they turn out to be much faster in the dense envelope cores where the density of ions is particularly low. Gas phase models predict centrally peaked radial distributions for SiS, CO, C_2H_2 and HCN, which come from the stellar atmosphere, and hollow shell distributions for C_2H, CN, and their products C_3H, C_4H, C_3N, HC_3N, etc..., which are formed in the envelope.

The first interferometric maps of molecular line emission in IRC+10216 were made by Bieging & Rieu (1988, 1989) with the Hat Creek mm array

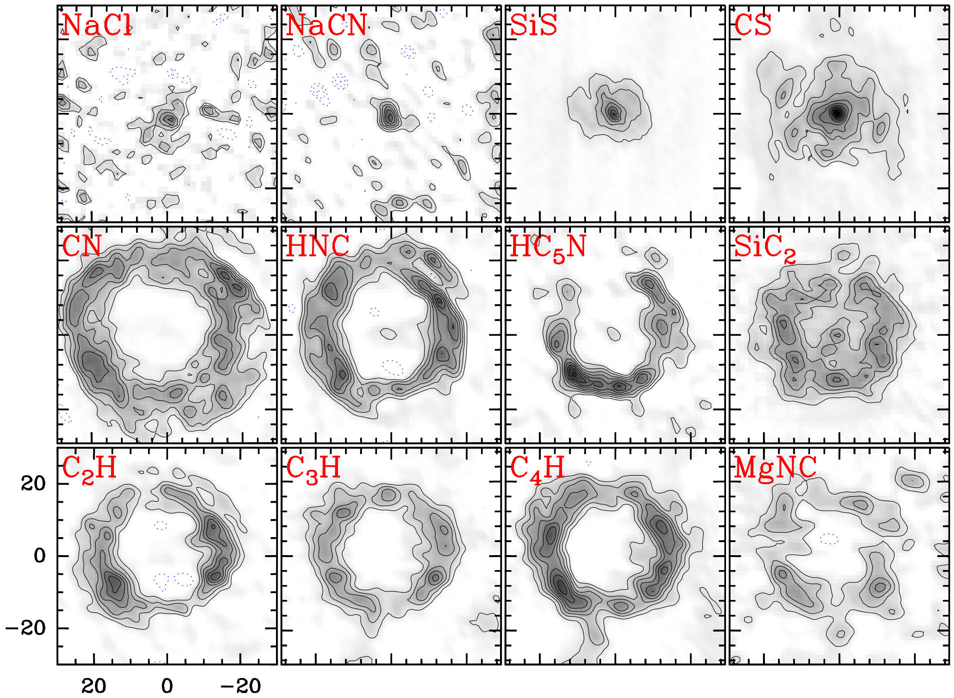

Figure 4. The IRC+10216 envelope, observed with an angular resolution of $\simeq 3''$ (FWHP) in the 3 mm lines of different molecules. The line intensities are integrated over the central 5 km s^{-1} interval (IRAM interferometer).

(HPBW $8''$). They nicely confirmed that the SiS emission was arising from a small central source and the HC_3N, HNC and C_2H emissions from hollow shells. They lacked, however, the resolution and sensitivity needed to resolve either the central SiS source or the structure of the shells. Further observations with the Hat Creek and Nobeyama arrays (Bieging & Tafalla 1993; Takano et al. 1992; Dayal & Bieging 1995) extended these observations to further species (SiC_2, CN, and C_4H).

The Plateau de Bure interferometer, which is more sensitive than the other mm arrays to small scale structures, is particularly well suited to study IRC+10216's dense core. A programme of mapping the chemically most significant molecules is under way with this instrument (Lucas et al. 1992; GLC; Lucas et al. 1995).

Figure 4 shows some examples of maps observed at Bure with a $\sim 3''$ synthesized beam. The emission is integrated over a 5 km s^{-1}–wide interval, centered on the source systemic velocity ($v_{\rm sys} = -26.4$ km s^{-1}). This interval was chosen narrow enough that the contours represent roughly the line brightness distribution in the meridian plane perpendicular to the line of sight (more exactly the surface brightness from a thin conical slab, since the envelope expansion velocity is roughly constant). The CN map results from a mosaic of 7 interferometer fields spaced by 20″ steps; the other are derived from single field observations and are not corrected for primary beam attenuation (HPBW$\simeq$ 50″). Some maps (CN, C_3H, C_4H, CS, SiC_2, and MgNC) include short spacing data, obtained by mapping the Bure field of view with the 30-m telescope; the others use only the central 30-m spectrum (HPBW 23″–27″). The continuum emission (essentially, a point-like source of flux 60 mJy) has been removed.

The maps in Fig. 4 confirm that the radicals and the cyanopolyynes have hollow-shell distributions (i.e. ring-like distributions in the velocity interval plotted in the figure) and that the small stable molecules are centrally peaked, as predicted by the gas-phase models. They show much more, however. First, the rings and the central sources show a rich azimuthal structure, in the form of thin arcs and clumps, with a crude axis of symmetry (see, e.g., the C_2H and SiS maps). Second, the rings show a radial structure suggesting the presence of double or even triple shells (e.g., the CN and C_2H maps). Third, some maps show at the same time a central source and a ring (CS and SiC_2). Fourth, the rings are off-centered by $\sim 2''$ to the E of the central star.

Most of the bright clumps are visible on several maps. Since the lines have different excitation conditions and opacities, the clumps cannot just be artifacts of the excitation and must trace an increase in column density. Similarly the decrease in intensity toward the N-NE and the S-SW (see C_2H) probably indicate a hole in the envelope.

According to gas phase models, the species in the envelope peak at different radii, since they are formed from different parent molecules through reactions with different time scales. For example, in Cherchneff et al.'s model (1993) C_4H is mainly formed by the neutral reaction $C_2H + C_2H$, whose characteristic time is $t = (k_n x(C_2H) n_{H_2})^{-1} \sim 2\,10^3$ yr, whereas C_3H is formed from C_2H, but by radiative association with C, a reaction at least 5 times slower. Neutral carbon, moreover, is abundant only in the outer envelope, further out than C_2H, so that the C_3H abundance is predicted to peak at a radius at least two times larger than C_4H. C_4H, itself, is predicted to peak at a radius ~ 1.5 times larger than C_2H (A. Glassgold, private communication).

This is not observed: the bright blobs in the C_2H, C_3H and C_4H maps (as well as in the maps of several species, such as MgNC–see GLC) coincide within 2″ (Fig. 2). This implies a time delay for the formation of C_3H and C_4H from $C_2H \leq 150$ yr, or a few percent of the characteristic reaction times! The peaks do not trace the envelope border, since CN and, mostly, CO extend further out. They do correspond to density clumps, but those are unlikely to be dense enough to reconcile the dynamical and chemical times, since they are not detected in ^{13}CO. Other examples of discrepancies between observations and predictions are the similarities between the CN and HNC distributions (Fig. 4) and the relatively small radius of the CN shell.

Clearly, the models, which assume spherical symmetry and a smooth density distribution, are much too crude in view of the complexity of the new data and attempts to model line excitation and gas phase chemistry in clumpy, asymmetrical media are required. Nonetheless, the above discrepancies probably ask for a reconsideration of the chemical networks.

It is tempting to see in the remarkable similarities between different species a common formation mechanism, capable of building large molecular abundances in timescales of few 10^2 yr. The gas density being a few times 10^4 cm^{-3} at $R = 15''$ and the abundance (relative to H_2) of the parent neutral species (C_2H_2, C_2H, HCN...) $x < 10^{-5}$, the reaction rates should be > a few times 10^{-9} cm^3 s^{-1}. This is faster than the Langevin rate and much faster than expected for neutral gas phase reactions. Photon-related processes, such as photodissociation and photodesorption from dust grains, on the one hand, and shock desorption of molecules weakly attached to grains, on the other hand, can be fast enough. What role they actually play in IRC+10216's complex chemistry, however, remains to be seen.

References

Bujarrabal, V., Alcolea, J. Neri, R., Grewing, M. 1994, Ap.J. 436, L169
Bieging, J.H., N-Q-Rieu 1988, Ap. J. 329, L107
Bieging, J.H., N-Q-Rieu 1989, Ap. J. 343, L25
Bieging, J.H., Tafalla, M. 1993, A. J. 105, 576
Cherchneff, I., Glassgold, A.E., Mamon, G.A. 1993, Ap. J. 410, 188
Dayal, A., Bieging, J.H. 1995, Ap. J. 439, 996
Guélin, M., Lucas, R., Cernicharo, J. 1993, in *The Cold Universe*, ed. Montmerle et al., Editions Frontières, Gif
Kastner, J.H., Weintraub, D.A. 1994, Ap. J. 434, 719
Kastner, J.H. 1992, Ap. J. 301, 337
Keady, J.J., Hall, D.N.B., Ridgway, S.T. 1988, Ap. J. 326, 832
Knapp, G.R., Morris, M. 1985, Ap. J. 292, 640
Loup, C., Forveille, T., Omont, A. and Paul, J.F. 1993, A&A Supp. Ser. 99, 377
Mamon, G., Glassgold, A.E., Huggins, P.J. 1988, Ap. J. 328, 797 (MGH)
Lucas, R., 1992 I.A.U. Symp. 150, p. 389
Lucas, R. et al. 1995, Ap. and Space Sience, 224, 293
Hajain, A., Phillips, J.A., Terzian, Y. 1995, Ap. J. 446, 244
Millar, T. J., Herbst, E. 1994, A&A 288, 561
Martin-Pintado, J. et al. 1995, Ap. J. 446, 687
Neri, R. et al. 1992, A&A 262, 544
Olofsson , H., Eriksson, K., Gustafsson, B., Carlstrom, U. 1993, Ap. J. *Supl* 87, 267
Ridgway, S.T., Keady, J.J. 1988, Ap.J. 326, 843
Sahai, R., Wannier, P.G. 1985, Ap. J. 299, 424
Shibata, K. et al. 1993, Ap. J. 415, 708
Takano, S., Saito, S., Tsuji, T. 1992, PASJ, 44, 469
Truong-Bach, Morris, D., Nguyen-Q-Rieu 1991, A&A 249, 435
Winters, J.M., Dominik, C., Sedlmayr, E. 1994, A& 288, 255
Walmsley, M. et al. 1991, 248, 555
Yamamura, I., Shibata, K., Kasuga, T., Deguchi, S. 1995, Ap. J. 427, 406.